

Global Magnetic Phase Diagram and Local Quantum Criticality in Heavy Fermion Metals

Qimiao Si^a,

^a*Department of Physics & Astronomy, Rice University, Houston, TX 77005-1892, USA*

Abstract

We address the global magnetic phase diagram of Kondo lattice systems. Through the distinct Fermi surface properties of the various phases at zero temperature, we argue that the phase diagram supports two classes of quantum critical point. One of these describes a direct transition from a magnetic metal phase with localized f -electrons to a paramagnetic one with itinerant f -electrons. This result provides the context for the picture of local quantum criticality, in which the Fermi surface jumps across the quantum critical point and the quasiparticle residue vanishes as the quantum critical point is approached from either side. Some of the unusual experiments, concerning the phases and quantum critical points of heavy fermion metals, are discussed from the present perspective. These developments have implications in broader contexts. In particular, they form a part of the growing evidence for quantum criticality that goes beyond the orthodox description in terms of order-parameter fluctuations.

Key words: quantum criticality, Fermi surface, non-Fermi liquid, heavy fermions
PACS: 71.10.Hf, 71.27.+a, 75.20.Hr, 71.28.+d

The past decade has witnessed the modern era in the study of heavy fermion metals. In part due to cross fertilization with studies on other classes of strongly correlated electron systems such as high temperature superconductors, the heavy fermions have become a prototype family of materials for non-Fermi liquid behavior [1,2] and quantum criticality [3,4,5]. One advantage that the heavy fermions have is that antiferromagnetic quantum critical points (QCPs) have been explicitly observed. The ensuing studies of the quantum critical heavy fermions have helped establish the notion that quantum criticality leads to both unconventional superconductivity and non-Fermi liquid behavior. Moreover, they have been instrumental in the growing realization that quantum criticality can be considerably more complex than its classical counterpart.

The universal properties of most classical critical points are described in terms of spatial fluctuations of an order parameter, $m(\mathbf{x})$. It is conventional wisdom

that a similar description applies to QCPs: the only change, reflecting the mixing of statics and dynamics, is that the order parameter fluctuations, $m(\mathbf{x}, \tau)$, are now in both space and imaginary time [6,7,8]. The experiments in heavy fermions have strongly contradicted this picture [2], pointing to emergent critical modes that are beyond the order-parameter fluctuations.

We have addressed this issue using microscopic approaches to Kondo lattice models [9,10,11,12,13,14], which have provided the basis for local quantum criticality. In this picture, Kondo screening turns critical at the magnetic quantum critical point. Here, we put the microscopic work in a more general context by considering the global magnetic phase diagram of the Kondo lattice. We show that there exist a number of metallic Fermi liquid phases, which are characterized by distinct Fermi surfaces. Different classes of QCP naturally occur in this phase diagram. Other theoretical approaches to the problem of quantum critical heavy fermions can be found in Refs. [15,16,17,18].

Email address: qmsi@rice.edu (Qimiao Si).

1. Global Magnetic Phase Diagram

We will focus on the Kondo lattice model,

$$H = H_f + H_c + H_K. \quad (1)$$

The Hamiltonian for the f -electron local moments is

$$H_f = \frac{1}{2} \sum_{ij} I_{ij}^a S_i^a S_j^a. \quad (2)$$

Here, $a = x, y, z$ are spin projections, and I_{ij}^a is the RKKY interaction between the spin-1/2 moments (one per site). We use I to label the typical RKKY interaction (say, the dominant component of the nearest-neighbor interactions), which is antiferromagnetic. In addition, G describes the degree of frustration (*e.g.* $G = I_{\text{nnn}}/I_{\text{nn}}$, the ratio of the antiferromagnetic next-nearest-neighbor interaction over the nearest neighbor one), or the degree of spatial anisotropy. For our purpose, it's adequate to know that increasing G corresponds to a decrease in the strength of the Néel order.

$$H_c = \sum_{\mathbf{k}\sigma} \epsilon_{\mathbf{k}} c_{\mathbf{k}\sigma}^\dagger c_{\mathbf{k}\sigma} \quad (3)$$

describes a band of conduction electrons – x per site, with $0 < x < 1$ without loss of generality. The bandwidth of the conduction electron is W . The two components interact with each other through

$$H_K = \sum_i J_K \mathbf{S}_i \cdot \mathbf{s}_{c,i}, \quad (4)$$

where the Kondo interaction, J_K , is antiferromagnetic.

The zero-temperature phase diagram can be specified in the multi-dimensional parameter space of x , I/W , J_K/W , and G . In a given material, the conduction electron density x is fixed, but the other parameters can be varied. Here, we will consider a fixed and (as in real materials) relatively small I/W .

In Fig. 1, the horizontal axis labels $j_K \equiv J_K/W$, while the vertical axis describes the local moment magnetism that is completely decoupled from the conduction electrons. When G is sufficiently large, the conventional Néel state becomes unstable towards states which preserve spin-rotational invariance but is translational-invariance breaking (spin Peierls) or preserving (spin liquid). We will not get into that regime, but will instead focus on the region of G where the local moment component itself remains in the Néel state. Still, incorporating the parameter G allows us to discuss the phase diagram beyond the traditional picture [19,20], which arises from considering only an energetic competition between the RKKY (I) and Kondo (J_K) couplings.

The magnetic phase diagram is shown in Fig. 1. The PM_L phase describes a heavy Fermi liquid with a Fermi

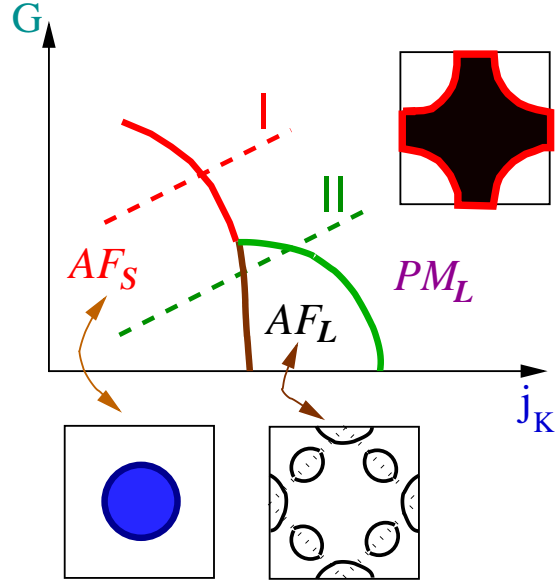


Fig. 1. The global magnetic phase diagram of the Kondo lattice at zero temperature. j_K is the Kondo coupling measured in terms of the conduction-electron bandwidth. G labels frustration. As illustrated, three phases, AF_S , AF_L and PM_L , have distinct Fermi surfaces. The dashed lines “I” and “II” label two types of transitions. More detailed descriptions are given in the main text.

surface that encloses $1+x$ electrons per unit cell within the paramagnetic Brillouin zone [21]. This phase can be most easily seen at $J_K/W \gg 1$, as illustrated in Fig. 2a. At each of the xN_{site} sites (where N_{site} is the number of unit cells in the system), a local moment and a conduction electron form a tightly bound singlet,

$$|s\rangle_i = (1/\sqrt{2})(|\uparrow\rangle_f |\downarrow\rangle_c - |\downarrow\rangle_f |\uparrow\rangle_c), \quad (5)$$

with a large binding energy of order J_K . Each of the remaining $(1-x)N_{\text{site}}$ sites hosts a lone local moment which, when projected to the low energy subspace, is written as

$$|\text{lone local moment } \sigma\rangle_i = (-\sqrt{2}\sigma)c_{i,\bar{\sigma}}|s\rangle_i. \quad (6)$$

In other words, if we consider the $|s\rangle$ as the vacuum state, a lone local moment behaves as a hole with infinite repulsion (there is only one conduction electron in the singlet) but with a kinetic energy of order W [22]. In the paramagnetic phase, we can invoke the Luttinger theorem to conclude that the Fermi surface encloses $(1-x)$ holes or, equivalently, $(1+x)$ electrons per unit cell. This is the heavy fermion state in which local moments, through an entanglement with conduction electrons, participate in the electron fluid [21]. The Fermi surface is large in this sense, and the phase is labeled as PM_L .

Another corner of the phase diagram where exact statements can be made is for $J_K/W (\ll I/W) \ll 1$.

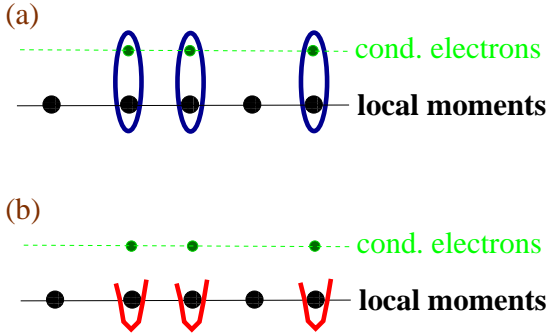


Fig. 2. (a) Kondo singlets and lone local moments in the $J_K \gg W \gg I$ limit; (b) In the opposite $J_K \ll I \ll W$ limit, static Kondo singlets do not form, but dynamical singlet correlations do exist.

For simplicity, we will consider the case with Ising spin anisotropy. The spin excitation spectrum of the Néel ordered local moment component is gapped; it follows that the Kondo coupling is irrelevant in the renormalization group sense. This is pictorially illustrated in Fig. 2b, where the Kondo coupling provides dynamical singlet correlation, but does not succeed in forming any “grip” (static Kondo singlet). Local moments stay charge neutral, and they do not contribute to the electronic excitations. The Fermi surface is small. We call this phase AF_S .

As the system moves from the AF_S phase to the PM_L phase, two things happen. First, the singlet correlation between the local moments and conduction electrons becomes stronger: when the “grip” finally forms, Kondo screening is realized. Second, the Néel order becomes more fragile and eventually goes away.

Traditionally, it is believed that the Kondo screening develops before the Néel order disappears. There is then an intermediate magnetically ordered state, in which the Fermi volume in the magnetic zone (for commensurate order) is the same as that of the AF_S phase. Nonetheless, the Fermi surface of this intermediate phase is labeled as large, in the sense that local moments have become a part of the electron fluid. This AF_L phase can be thought of as a spin-density-wave (SDW) state formed out of the heavy fermion quasiparticles of the PM_L phase; indeed, the Fermi surface of the AF_L phase is adiabatically connected to that of PM_L , when the magnetic order parameter is switched off. This Fermi surface of the AF_L phase has a different topology from that of the AF_S phase (as can be most easily seen near the multicritical point); the two phases are separated by a Lifshitz transition. The magnetic quantum transition is between the AF_L and PM_L phases, and is labeled type II.

It is also possible, however, for a direct transition between the AF_S and PM_L phases. This is the type I transition shown in Fig. 1.

2. Quantum Critical Points

At the type II magnetic transition, the effective Kondo screening scale of the lattice – the coherence temperature – is finite. The quantum critical point belongs to the Hertz-Moriya-Millis type [6,23,24].

The type I magnetic transition, however, goes directly from the AF_L phase to the PM_L phase. The transition is second order if z_L , the quasiparticle residue of the large Fermi surface in the PM_L phase, and z_S , its counterpart of the small Fermi surface in the AF_S phase, go to zero as the transition is reached from respective sides. The coherence temperature vanishes – and the Kondo singlets disintegrate – as the QCP is approached from the PM_L side.

At such a magnetic QCP, the destruction of Kondo screening coincides with the onset of magnetic ordering. The understanding of actually how the quasiparticles are destroyed at the QCP comes from microscopic considerations. One mechanism is the local quantum criticality [9,10,11,12].

Fluctuations of the magnetic order parameter are the softest at the magnetic QCP. These slow fluctuations in turn decohere the Kondo screening, making the Kondo effect critical. The latter characterizes the emergent non-Fermi liquid critical excitations, which are in addition to the critical fluctuations of the magnetic order parameter.

The local QCP has a number of characteristics. Electronically, the f -electrons turn from being itinerant to being localized across the QCP. There are two corollaries. The Fermi surface undergoes a sudden reconstruction at the QCP. In addition, the continuous vanishing of both z_L and z_S implies that the effective mass diverges as the QCP is approached from both the paramagnetic and magnetic sides. It is worth expanding on this feature for the magnetic side. The mass enhancement in heavy fermions has traditionally been associated with the formation of Kondo resonance. How can the AF_S phase, having no Kondo resonance, acquire small quasiparticle residue and large effective mass? As Fig. 2b illustrates, here, even though Kondo singlet is not formed in the static sense, dynamical singlet correlation does occur and becomes stronger as the QCP is approached. It is this dynamical effect that enhances both the thermodynamic mass (as measured in, *e.g.*, specific heat coefficient) and electronic mass (as measured in, *e.g.*, dHvA).

A second feature of the local QCP arises in the magnetic dynamics. In contrast to the Gaussian fixed point of the $T = 0$ SDW transition, where ω/T scaling is violated [6,23,24], the interacting nature of the local QCP produces an ω/T scaling. Moreover, the magnetic dynamics contains a fractional exponent. The dynamical spin susceptibility turns out to have the form [9,10,12]

$$\chi(\mathbf{q}, \omega) = \frac{\text{const.}}{I_{\mathbf{q}} - I_{\mathbf{Q}} + (-i\omega)^{\alpha} M(\omega/T)}, \quad (7)$$

where \mathbf{Q} is the antiferromagnetic ordering wavevector.

3. Experiments

Experimental data in heavy fermions suggest that both the antiferromagnetic and paramagnetic phases are indeed Fermi liquids. In YbRh_2Si_2 , for instance, the resistivity is T^2 on both sides of the QCP [5]. Related features have been observed in CePd_2Si_2 [25,26] and $\text{CeCu}_{6-x}\text{Au}_x$ [3]. In the case of $\text{CeCu}_{6-x}\text{Au}_x$, for $x > \sim x_c$ with small T_N , however, the specific heat coefficient does not appear to saturate at the lowest measured temperatures; this region remains to be clarified.

There are also extensive Fermi surface measurements via dHvA. It is well established that the paramagnetic metal phase has a large Fermi surface [27]. Perhaps less well known is the fact that antiferromagnetic heavy fermions are typically found to have a small Fermi surface (for recent reviews, see Ref. [28]). Since a large magnetic field – which is a big perturbation to heavy fermions – is necessarily involved in the experiment, it is natural that the dHvA measurement generically probes the parts of the phase diagram sufficiently away from the magnetic-transition region. By extension, it is natural that the AF_S and PM_L phases are the ones that are commonly identified in such measurements.

We now turn to experiments which zoom in on the transition region. Consider first the inelastic neutron scattering experiments. $\text{CeCu}_{6-x}\text{Au}_x$, at $x = 0.1 \approx x_c$, is the most striking case of a single crystal showing a dynamical spin susceptibility with a fractional exponent and an ω/T scaling, of the form given in Eq. (7) [29,30].

Recent measurements [31] have been carried out in $\text{Ce}(\text{Ru}_{1-x}\text{Rh}_x)_2\text{Si}_2$. This single crystal displays a paramagnetic to antiferromagnetic metal transition at $x_c \approx 0.04$. Close to this concentration, the inelastic neutron scattering data is well described by the Lorentzian form, $\chi(\mathbf{q}, \omega) = \chi_{\mathbf{q}}(T)/[1 - i\omega/\Gamma_{\mathbf{q}}(T)]$, with $\Gamma_{\mathbf{Q}} \sim T^{3/2}$. This form, violating ω/T scaling, is what is expected in a 3D AF SDW QCP [6,23,24]. In addition, the electrical resistivity and specific heat data are also reasonably consistent with the SDW picture. While it will be important for future experiments to map out the T_N line closer to the $T = 0$ transition (the lowest finite T_N that has been determined so far is of the order of 3 K), the evidence seems quite strong that we are finally seeing a Hertz QCP! Unlike the quasi-2D nature [30,29] seen in $\text{CeCu}_{6-x}\text{Au}_x$, the magnetic fluctuations in $\text{Ce}(\text{Ru}_{1-x}\text{Rh}_x)_2\text{Si}_2$ are three-dimensional [31]. This makes $\text{Ce}(\text{Ru}_{1-x}\text{Rh}_x)_2\text{Si}_2$ to be located at the lower part of our global phase diagram (Fig. 1) than $\text{CeCu}_{6-x}\text{Au}_x$. This placement is consistent with the

identification of type II and type I quantum transitions in these two materials, respectively.

Consider next electronic measurements in the immediate vicinity of the transition. Detailed Hall effect studies [32] have been carried out in YbRh_2Si_2 . In this material, the anomalous Hall component is relatively small at low temperatures, allowing the extraction of the normal Hall component. The Hall coefficient shows a rapid crossover at finite temperatures, extrapolating to a jump in the $T = 0$ limit at the magnetic QCP. The result provides strong evidence that the second order quantum transition in YbRh_2Si_2 goes directly from AF_S to PM_L.

We already mentioned that the large magnetic field needed in dHvA makes it generally difficult to use this method to zero in on the quantum critical point. A fortuitous situation arises in CeRhIn_5 . A magnetic field, of the order used in the dHvA measurement, is just what is needed to entirely suppress superconductivity and expose a pressure induced zero-temperature transition from an antiferromagnetic metal to a paramagnetic metal [33]. Indeed, the dHvA result [34] can be interpreted in terms of a sudden reconstruction of Fermi surface, from that of AF_S to its counterpart of PM_L, across the critical pressure. Moreover, the (electronic) dHvA mass shows a large (more than 10-fold) increase as the QCP is approached. Taken together, these measurements provide strong evidence for a field- and pressure-induced type I magnetic QCP in CeRhIn_5 .

Finally, some thermodynamic ratios also turn out to be illuminating in this context. We have shown in Ref. [35] that the Grüneisen ratio Γ – the ratio of the thermal expansion, $\alpha \equiv \frac{1}{V} \frac{\partial V}{\partial T}$, over the specific heat, c_p – has to diverge at any QCP where the control parameter is linearly coupled to pressure. Scaling implies that, at the QCP, $\Gamma \sim 1/T^x$, with the exponent $x = 1/z\nu$ (where z is the dynamic exponent and ν the correlation length exponent). Measurement [36] in YbRh_2Si_2 does indeed find such a divergence. Moreover, the exponent $x \approx 0.7$ is different from the value (1) expected from an AF SDW QCP, but is consistent with the value calculated from the local QCP picture.

4. Summary and Outlook

We have shown that two types of magnetic metal phases - AF_S and AF_L - can occur in Kondo lattices, along with the standard heavy fermion paramagnetic metal phase PM_L. This opens up a new type of magnetic quantum phase transition, which goes directly from AF_S to PM_L. The transition is second order when quasiparticle residues vanish. At this magnetic QCP, the critical excitations include not only the fluctuations of the order parameter but also those associated with

a critical Kondo screening. Local quantum criticality is one form of such type of QCP.

We close with a few general remarks. The global phase diagram makes it desirable to systematically study magnetic quantum transitions in heavy fermion metals with different degrees of frustration. For instance, YbAgGe has a hexagonal lattice and its spin interactions may very well be frustrated. Indeed, the magnetic phase transitions in this material are rather unusual [37]. The venerable UPt₃ also has a hexagonal lattice and it could be instructive to study quantum phase transitions in this material or its relatives.

The prominent role played by the destruction of Kondo screening in our global phase diagram has other implications. We may, for instance, replace the Néel order parameter discussed so far by a spin glass one. We are then led to two types of quantum spin glass transitions. The type II transition (SG_L to PM_L) is expected to be described by a Gaussian fixed point [38,39], with a violation of ω/T scaling in the magnetic dynamics. A type I transition (SG_S to PM_L), on the other hand, can correspond to an interacting fixed point, yielding an ω/T scaling. Recent inelastic neutron scattering study [40] near a spin-glass QCP of Sc_{1-x}U_xPd₃ [41] does indeed find an ω/T scaling and a fractional exponent, suggesting a destruction of Kondo screening at this spin-glass QCP. The striking similarity of these data with those of UCu_{5-x}Pd_x [42,43] naturally suggests that the later too originate from a destruction of Kondo screening at a spin-glass QCP.

Finally, it is possible that the physics of magnetic quantum criticality with critical Kondo screening in heavy fermion metals connects to that of certain quantum critical spin liquid states in quantum insulating magnets [44,45,46]. Itinerant systems such as heavy fermions are inherently spin-1/2 systems. This is in contrast to insulating magnetic materials, in which the size of spin is typically larger than 1/2, making quantum effects less pronounced. So, perhaps, heavy fermion metals can also play an important role in the on-going search for both critical and stable spin liquid states.

I am particularly gratefully to D. Grepel, K. Ingersent, S. Kirchner, E. Pivovarov, S. Rabello, J. L. Smith, J.-X. Zhu, and L. Zhu for collaborations in this area, and many colleagues for discussions. The work has been partially supported by NSF Grant No. DMR-0424125 and the Robert A. Welch Foundation.

References

- [1] M. B. Maple *et al.*, J. Low Temp. Phys. **95** (1994) 225.
- [2] G. R. Stewart, Rev. Mod. Phys. **73** (2001) 797.
- [3] H. v. Löhneysen *et al.*, Phys. Rev. Lett. **72** (1994) 3262.
- [4] N. D. Mathur *et al.*, Nature **394** (1998) 39.
- [5] J. Custers *et al.*, Nature **424** (2003) 524.
- [6] J. A. Hertz, Phys. Rev. B **14** (1976) 1165.
- [7] P. Pfeuty, Ann. Phys. N.Y. **57** (1970) 79.
- [8] A. P. Young, J. Phys. C **8** (1975) L309.
- [9] Q. Si *et al.*, Nature **413** (2001) 804.
- [10] D. R. Grempel and Q. Si, Phys. Rev. Lett. **91** (2003) 026401.
- [11] J.-X. Zhu *et al.*, Phys. Rev. Lett. **91** (2003) 156404.
- [12] Q. Si *et al.*, J. Phys.: Condens. Matter **17** (2005) R1025.
- [13] P. Sun and G. Kotliar, Phys. Rev. Lett. **91** (2003) 037209.
- [14] P. Sun and G. Kotliar, Phys. Rev. B **71** (2005) 245104.
- [15] P. Coleman and C. Pépin, Acta Physica Polonica **B34** (2003) 691.
- [16] C. Pépin, Phys. Rev. Lett. **94** (2005) 066402.
- [17] J. Rech *et al.*, cond-mat/0507001.
- [18] T. Senthil *et al.*, Phys. Rev. B **69** (2004) 035111.
- [19] S. Doniach, Physica **B91** (1977) 231.
- [20] C. M. Varma, Rev. Mod. Phys. **48** (1976) 219.
- [21] N. E. Bickers, Rev. Mod. Phys. **59**, 845 (1987).
- [22] C. Lacroix, Solid State Commun. **54** (1985) 991.
- [23] T. Moriya, *Spin Fluctuations in Itinerant Electron Magnetism* (Springer, Berlin, 1985).
- [24] A. J. Millis, Phys. Rev. B **48** (1993) 7183.
- [25] F. M. Grosche *et al.*, J. Phys. Cond. Matt. **13** (2001) 2845.
- [26] A. Demuer *et al.*, J. Phys. Cond. Matt. **13** (2001) 9335.
- [27] L. Taillefer and G. Lonzarich, Phys. Rev. Lett. **60** (1988) 1570.
- [28] A. McCollam *et al.*, Physica **B359** (2005) 1; Y. Ōnuki *et al.*, Acta Physica Polonica **B34** (2003) 667.
- [29] A. Schröder *et al.*, Nature **407** (2000) 351; Phys. Rev. Lett. **80** (1998) 5623.
- [30] O. Stockert *et al.*, Phys. Rev. Lett. **80** (1998) 5627.
- [31] H. Kadowaki *et al.*, cond-mat/0504386.
- [32] S. Paschen *et al.*, Nature **432** (2004) 881.
- [33] T. Park *et al.*, preprint (2005).
- [34] H. Shishido *et al.*, J. Phys. Soc. Jpn. **74** (2005) 1103.
- [35] L. Zhu *et al.*, Phys. Rev. Lett. **91** (2003) 066404.
- [36] R. KÜchler *et al.*, Phys. Rev. Lett. **91** (2003) 066405.
- [37] S. L. Bud'ko *et al.*, Phys. Rev. B **71** (2005) 054408.
- [38] S. Sachdev *et al.*, Phys. Rev. B **52** (1995) 10286.
- [39] A. M. Sengupta and A. Georges, Phys. Rev. B **52** (1995) 10295.
- [40] S. Wilson *et al.*, Phys. Rev. Lett. **94** (2005) 056402.
- [41] D. Gajewski *et al.*, Phys. Rev. B **62** (2000) 5496.
- [42] M. C. Aronson *et al.*, Phys. Rev. Lett. **75** (1995) 725.
- [43] D. E. MacLaughlin *et al.*, Phys. Rev. Lett. **87** (2001) 066402.
- [44] T. Senthil *et al.*, Science **303** (2004) 1490.
- [45] Q. Si, *Advances in Solid State Physics* **44** (2004) 253; cond-mat/0404303.
- [46] T. Senthil *et al.*, Physica **B359** (2005) 9.